Space-time pressure distribution applied to a stiff concrete structure through a protective sand layer from full-scale experimental rock fall tests

Bruna Garcia, Tarik Oussalah, Jean-Pierre Rajot, Anne-Sophie Colas

SPACE-TIME PRESSURE DISTRIBUTION APPLIED TO A STIFF CONCRETE STRUCTURE THROUGH A PROTECTIVE SAND LAYER FROM FULL-SCALE EXPERIMENTAL ROCK FALL TESTS

Bruna Garcia1, Tarik Oussalah1, Jean-Pierre Rajot1, and Anne-Sophie Colas1

1Université Gustave Eiffel, Département GERS, Laboratoire RRO, 25 avenue François Mitterand, Case 24 Cité des mobilités. F-69675 Bron, Email: jean-pierre.rajot@univ-eiffel.fr

Abstract

This study focuses on the characterization of low-velocity (lower than 100 km/h) rockfall impact loads transferring to a thick steel-reinforced concrete (SRC) slab through a protective sand layer. A full-scale experimental tests campaign was performed, each test consisting in releasing a concrete block which, after a vertical free-fall, impacts a sand protective layer placed over a SRC slab, in order to represent an isolated rockfall impact to which an actual SRC structure could be exposed. During the impact, the vertical pressure distribution was observed using several pressure cells installed at the sand-slab interface. A total of 35 tests were carried out, systematically combining sand layer thickness (D), block's equivalent diameter (B), and free-fall drop height (H), related to impact velocity. The masses of the released blocks were in the range of 117 to 7399 kg, corresponding to diameters in the range of 0.42 to 1.79 m. Five free-fall drop heights, up to 33 m, were considered, to reach impact velocities up to 90 km/h, covering the range of most velocities observed in actual rockfall studies. Three thicknesses of the sand layer protecting the thick SRC slab were considered: 1, 1.5 or 2 m. Data reduction from this full-scale impact tests program makes it possible to characterize, for a given thickness of protective sand layer, the time-space pressure pulse distribution applied to the protected structure during the impact for a large range of rock boulder masses and speeds actually observed in the field.

INTRODUCTION

Among the possible rockfall protections, various types of steel meshes devices have been developed to mitigate rockfalls of low to medium impact energy (1 to 10 MJ). Rockfall shed galleries (Figure 1) or, when adapted to the site profile, reinforced soil bunds are being used for medium to large energy levels. To improve the durability and maintenance of these structures, which are often critical for infrastructure operation and rescue organization, granular soil layers may be placed on the roof of rock-shed galleries, tunnel heads or other structural elements possibly exposed to direct hit from a falling rock boulder.

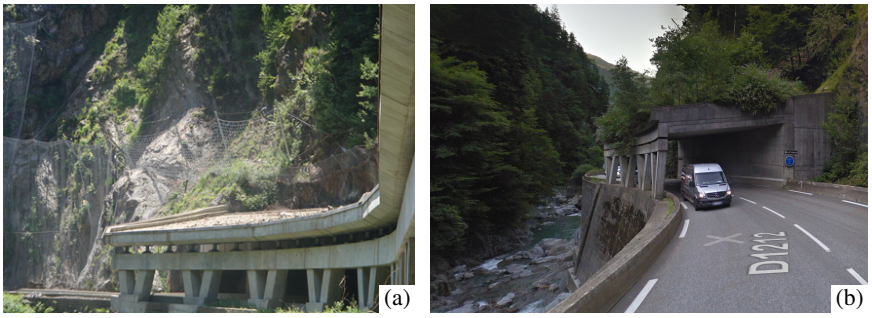

Fig. 1. Example of a rock shed gallery in Val d'Arly (Ugine, French Alps).

Granular soils are often available and their performance to protect structures from rockfall impacts, although not yet fully quantified, has been demonstrated for ages. Without a protective granular soil layer, the collision with the rock boulder produces significant damages to the steel reinforced concrete structure to dissipate a large amount of energy within a very short period of time (Durville et al. 2010). When a soil layer is protecting the structure, large deformations and displacements occur in the soil during the impact, which dissipates part of the energy. The impact load is then transmitted to a wider surface of the structure and is applied more progressively and during a longer period, resulting in a lower damage to the structure.

In fact, analysis of the dynamic penetration of a rock boulder in soils, eventually with subsequent soil-structure interaction during penetration, raises several major issues for predictive numerical modeling. As a consequence, many authors rather developed experimental approaches to investigate the physical phenomena and propose empirical relationships. In the literature, a significant number

of reduced-scale tests have been performed to investigate the influence of several factors, such as block's mass, block's shape, impact velocity, angle of impact, protective soil grain size distribution, relative density, thickness of the layer, etc. The majority of analytical or empirical expressions derived from these tests give an estimate of the maximum impact force at the top of the protective soil layer, but not to the force transmitted to the structure at the soil-slab interface.

Based on their reduced scale tests, some authors (Yoshida et al. 1988; Montani Stoffel 1998; Heidenreich 2004; Calvetti and Di Prisco 2012; Schellenberg 2008) proposed empirical relationships to estimate the maximum value of the impact force and the block's penetration depth. They also considered the maximum value of the forces transmitted to the protected structure and to its foundation, which may differ from each other due to structural dynamic effects during impact. Other research results on dynamic structural design remain confidential, due to private-company led research or to their potential military use.

Two of the most important design guidelines for rockfall protective soil layers are the Japanese Rockfall Countermeasures Handbook (Japan Road Association 2000) and the Swiss Technical Guide (ASTRA – Swiss Federal Transportation Office 2008). Based on the empirical relationships for the maximum value of the impact force and for the block penetration depth, these guidelines suggest recommendations to define the equivalent pressure distribution transferred through the protective layer to be considered in quasi-static design analysis of the structure. These guidelines also include requirements on the layer thickness to prevent the rock boulder from reaching the structure during an impact.

Still, several authors (Bhatti 2015; Pichler et al. 2005; Labiouse et al. 1996; Schellenberg 2008; Calvetti and Vecchiotti 2005; Kishi et al. 2002) pointed out the lack of full-scale tests to extrapolate these empirical expressions to actual rock block sizes and impact energies of the order of those observed in the field. In fact, in dynamics, inertia forces involve both the space-scale and the time-scale, which therefore does not allow to define an unique similarity relationship between reduced-scale tests and the full-scale impacts in the field. Furthermore, for dynamic mechanical analysis of the protected structure, not only an equivalent quasi-static maximum value of the load

transferred to the structure through the soil layer is needed, but the time-rate and duration of the loading, as well as its spatial distribution, are of crucial importance because the inertia of the structure has a significant influence on the stress values actually applied to its constitutive materials during impact. The main objective of the present study is to propose a method to characterize the space-time pressure pulse distribution applied to a structure protected by a sand cushion layer during an impact from a rock boulder. This distribution may be directly used by the structural engineer for the dynamic design of the structure. For that purpose, an extensive full-scale experimental parametric study was performed to characterize how impact loads of low-velocity (lower than 100 km/h), from boulders of various sizes, are transmitted through a protective sand layer of given thickness (Oussalah 2018). In those tests, the focus was therefore on the measurement of the pressure at the interface between the protective sand layer and the structure. One assumption was however made concerning the choice of impact condition factors to be varied in the experimental program. Among the numerous factors which may affect the pressure distribution transmitted to the protected structure during impact, three impact condition factors were assumed to have the most significant influence on the pressure pulse: (1) The thickness of the protective soil layer (D), (2) The impacting boulder size (B), assuming a spherical block of equivalent diameter related to its mass (considering an average rock density for most rocks) and (3) The impact velocity (V), considering a trajectory normal to the roof of protected structure. Like for the assumed large stiffness of the protected structure, a normal angle of impact was considered to produce the largest pressures at the soil-structure interface compared to lower impact angle values, thus safely overestimating the normal pressure pulse to be considered in the dynamic structural design. The reader interested in the discussion on the main impact condition factors can refer to the first chapter of Oussalah (2018).

METHODOLOGY

Experimental tests

Experimental full-scale rockfall testing facility

The major equipment of the Gustave Eiffel University experimental rockfall testing station is a tower crane jib installed at the top of a 70 m high vertical cliff. Loads of up to 200 kN (masses of

about 20 tons) can be lifted and released using an electrohydraulic hook equipped with a damping device.The maximum impact velocity is about 133 km/h and the maximum impact energy of the order of 13.5 MJ.

Finally, a precast slab, named Slab 1 in Fig. 2(a), is located on the ground level platform. Slab 1 is composed of steel reinforced concrete (SRC), having 60 cm thick embedded in the rock substratum. It is 4.5 m wide and 8 m long and was used in this study to simulate a very stiff structure protected by a sand layer which would be impacted by a boulder.

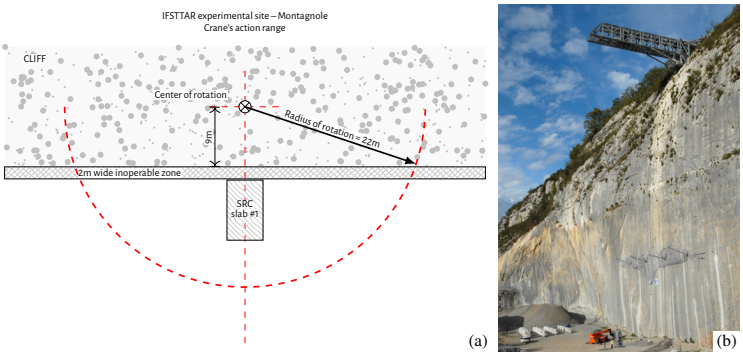

Fig. 2. Schematic plan view (a) and picture (b) of the Gustave Eiffel's full-scale rockfall experimental testing facility in Montagnole, France.

Sand classification and protective soil layer construction procedure

Only one type of granular protective material was considered in this experimental campaign: a rolled and clean alluvial sand to guarantee that the material remains cohesionless for a long period of time after its placement. Figure 3 shows the grain size distribution of the clean rolled sand used in this study. Soil particle sizes range from 0 to 4 mm and the fraction passing the 80 μm sieve represents 3.5% in mass.

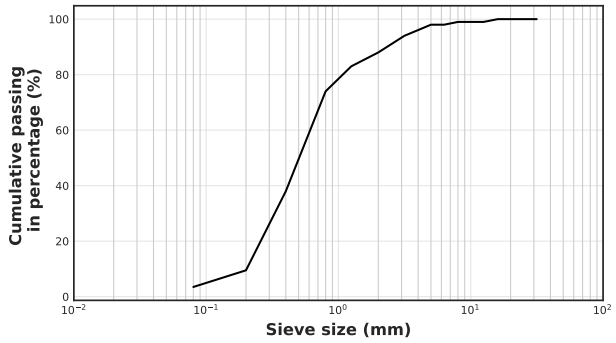

Fig. 3. Grain size distribution of the sand used in the study.

Figure 4 illustrates the construction of the sand cushion layer over the reinforced concrete slab. As shown in Fig. 4(a), a geotextile was first placed on the slab and surrounding ground surface The sand cushion layer was placed in successive sub-layers, each one of 40 cm thick (b) and compacted by three passes of a vibrating plate compactor (model MVCF60 – Mikasa) at the maximum traveling speed of about 25 m/min, alternating converging and diverging spiral paths (c).

Fig. 4. (a) Soil dumping on geotextile using a backhoe; (b) Leveling of the soil sub-layers and (c) soil compaction using a vibrating plate compactor.

The soil's stiffness has a presumably influence on the pressure transmitted to the protected structure. To reduce the scope of the parametric study to the three impact condition factors D, B and V, all the tests were performed on the sand cushion layer compacted to the same dry density of about 1.53. After each test, being disturbed by the impact and penetration of the boulder, the sand was removed and the protective sand layer was constructed again, applying the same construction procedure. During construction, the homogeneity of compaction was controlled with in-situ PANDA dynamic penetrometer profiles and the unit weight of the compacted sand was determined applying

the in-place measurement method defined in the NF P 94-061-4 standard.

Instrumentation

Instrumentation included two high-speed cameras (1000 images per second), a triaxial accelerometer attached to the impacting block and seven pressure cells installed on the upper surface of the horizontal SRC slab,before placing the sand layer. measurements were synchronized and recorded at an acquisition frequency of 10 kHz.

Figure 5(a) shows one of the pressure cells used in the experimental tests (Model 3515-1 from GEOKON). Strain gauge sensors are well suited for the high frequency data acquisition required in this study. Depending on the cell model type, the measured pressure may range from 0 to 1.5, 3 or 6 MPa, with an accuracy of 0.25% of the full scale range.

The seven pressure cells were installed forming an "L" shape at the slab's upper face (see Figure 5(b) and Figure 7). They were sealed to the slab with quick-setting cement and covered with a plastic film to protect them from water infiltration during the in-situ testing period. The right angle of this "L", at the center of the slab, was the targeted impact point. The impact test conditions being axisymmetric, the "L" shape was devised to check for possible side effects and introduce some redundancy in the data.

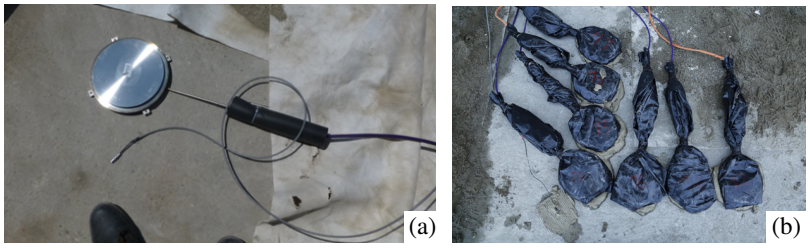

Fig. 5. Granular soil pressure cell (a), installed in an "L" shape on the slab's upper face (b).

Full-scale testing program

Table 1 describes the referencing system used to identify each of the three varied impact conditions factors D, B and V (related to the free fall height of the boulder (H)). An index from 1 to 5 was used to designate in each test the layer thickness, the boulder size and the impact velocity. For example, test D2B2H3C2 corresponds to the test where the layer thickness D is equal to 1.5 m, the

equivalent block diameter B is 0.73 m and drop height is 10 meters (impact velocity (V) of 50.4 km/h). C2 refers to the layer compaction procedure, the same for all the tests. Figure 6 shows the

Table 1. Tests referencing for the different impact conditions factors values.

Index	Sand cushion layer thickness D (m)	Boulder diameter B (m)	Free-fall height H (m)	Impact speed V (m/s)	Impact speed V (km/h)
1	1	0.42	1	4.43	16.0
2	1.5	0.73	5	9.90	35.6
3	2	0.73	10	14.00	50.4
4	–	1.54	20	19.81	71.3
5	–	1.78	33	25.45	91.6

five different impacting blocks used in the tests. The first two blocks are spherical, composed of a steel shell filled with concrete. The three other blocks, with a rhombicuboctahedral shape, are made of steel fiber-reinforced concrete. They were conventionally designed for the full-scale rockfall tests required for the European Certification of Rockfall Protection Kits. Table 2 gives the characteristic

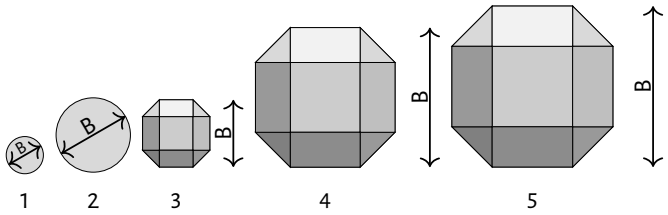

Fig. 6. Characteristic dimension of impacting blocks referenced from 1 to 5.

properties of each block. In order to represent a similarity to real impacting boulders, the unit mass of all blocks was close to that of most rocks (2500 kg/m^3). For the last three impacting blocks, B takes the value of the equivalent sphere having exactly the same mass, by assuming an unit mass of 2500 kg/m^3. It may be noted that the mass of Block 2, of spherical shape, is close to that of block 3, of rhombicuboctahedral shape. These two blocks were used to investigate the influence of the blocks shapes on the observed pressure pulse. In the range of protective layer thicknesses and impact velocities considered in this study, no significant influence of the block shape was identified. Thus, as far as transmission of pressure pulse through a sand layer is concerned, blocks with

Table 2. Impacting blocks characteristics and equivalent diameter (B)

Block index	Unit Mass (kg/m^3)	Block Mass (kg)	Block diameter B (m)
1	2500	117	0.42
2	2500	553	0.73
3	2500	543	0.73
4	2500	4796	1.54
5	2500	7399	1.78

rhombicuboctahedral shape may reasonably be considered as spherical with equivalent diameter B, for the range of impact condition factors considered in this study (see chapter 5 of Oussalah (2018), page 161).

In Appendix I, for each of the 35 tests performed in this study, Table 3 indicates the impact condition factors D, B and V according to the referencing convention.

Experimental set-up

Figure 7 is a schematic representation of the test's set-up and instrumentation plan. A coordinate system was defined, where the origin is at the slab center, the positive x-axis in the direction of the slab's largest dimension (towards the cliff), the positive y-axis in the direction of the slab's width and the z-axis upwards vertical. The cross-section AA' includes the three impact test condition factors D, B and H (the free-fall height, related to impact speed V) and their respective sets of values in the experimental program.

For all sand cushion layer thicknesses, the extend of the protective fill at the ground level was such that the top surface would be centered on the slab and no less than 7 m long (in the x-direction) by 4 m wide (in the y-direction) to avoid possible boundary effects when the boulder hits the center of the test's set-up. Axisymmetric mechanical conditions were checked comparing the pressure measurements on the slab in both x and y directions.

In Figure 7(b) and (c), the two plan views refer to the two configurations of the seven pressure cells locations (in red in the figure, numbered 11 to 17) which were used in the experimental pro-

gram, called “Config1” and “Config2” in the figure. In Figure 7(b), and for Config1, the spacing between the centers of two adjacent pressure cells (of diameter 23 cm) was the same in both the x and y directions, equal to 25 cm. In Config2 (Figure 7(c)), the spacing between the centers of two adjacent pressure cells was, in the direction of the fill length (x-direction), 40 cm and, in the direction of the fill width (y-direction), 50 cm.

The first configuration was used for the tests with the smallest cushion layer thickness (D = 1 m) while the second for the two larger thicknesses (1.5 or 2 m), to account for possible wider diffusion of the forces as the thickness of the sand cushion increases. The pressure cells were placed along two directions from the center of the slab to provide some redundancy in the measurements and to check the assumption of axisymmetric loading conditions. Finally, two high-speed cameras (C#1 and C#2 in the figure) were installed in two horizontal directions.

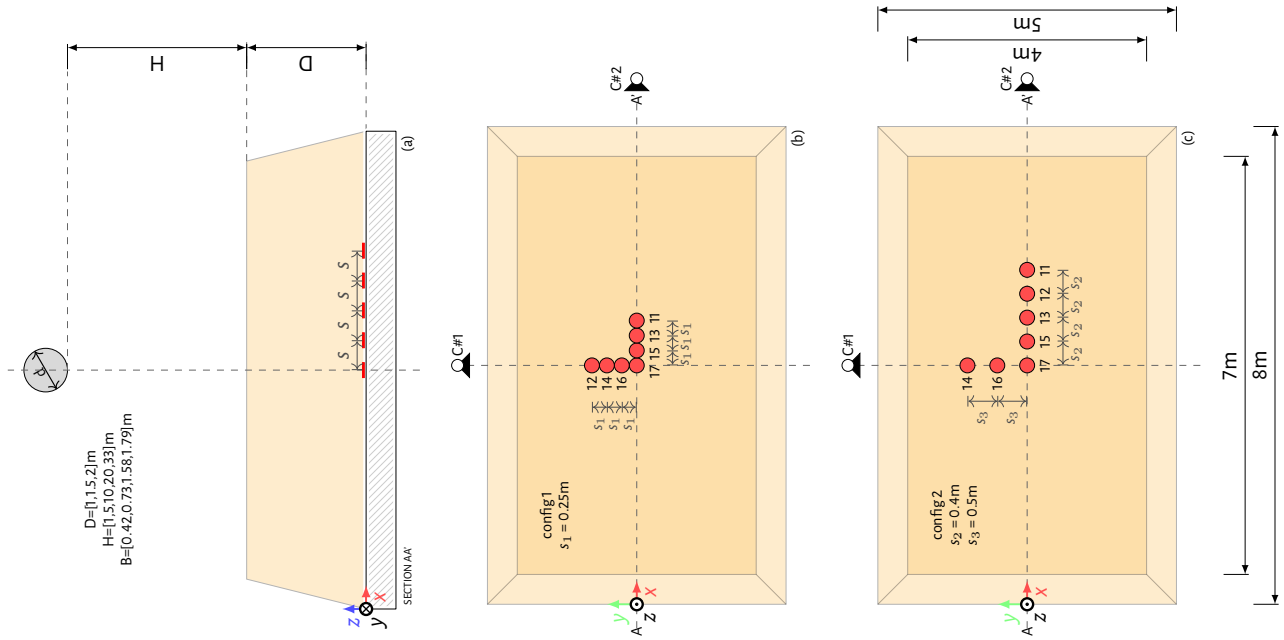

Fig. 7. Schematic representation of test setup and instrumentation plan. (a) AA’ cross-section; (b) and (c) are the plan view for the two pressure cells spacing configurations (Config 1 and Config 2, respectively).

Data reduction

Corresponding to a vertical impact on a horizontal homogeneous fill protecting a concrete slab, the impact test conditions were presumably axisymmetric. The pressure measurements at the top of the slab were therefore analyzed in terms of time (t) and horizontal (radial) distance (r), at the slab surface, from the vertical impact trajectory to the centers of the different pressure cells.

The block was lifted from the targeted impact point at the top surface of the fill, located just above the P17 pressure cell at the right angle of the L-shaped pressure cells set-up. In fact, it turned out that, due to the electrohydraulic hook dropping mechanism, during the test the actual impact point observed on the high speed video recordings might be a few centimeters away from the targeted impact point. In addition, although test conditions were axisymmetric by principle, a slight deviation of the boulder (a few more centimeters in the horizontal direction over the penetration depth) was systematically observed during its penetration in the sand fill.

As a consequence, for the sake of analyzing the results from a series of tests which basically were axisymmetric, the location of the vertical impact trajectory was deemed to be defined by the center of the boulder at the end of the test. For that purpose, the exact position of the block after penetration in the sand fill was determined by triangulation using measured distances from the top of the block to two referenced points sealed in the cliff. In Appendix I, Table 3 includes the values of these two impact coordinates, denoted X_{impact} and Y_{impact}. Figure 8 is a schematic representation of a test configuration after impact. As explained previously, in the plan view the location of the free-fall impact trajectory is defined by the center of the boulder after penetration. In the horizontal plane at the slab level, the radial distances of the pressure cells numbered P_{1i}, i = 1 to 7, were denoted $r_{(P_{1i})}$.

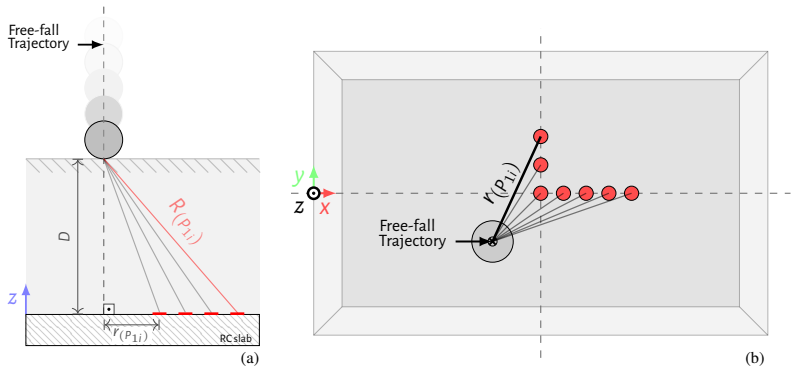

Fig. 8. Schematic representation of distances from impact trajectory to the pressure cells.

The beginning of an impact was considered to be the moment when the block immediately touches the protective layer. This location of the block, at the top of the layer on the vertical impact trajectory, defines the initial distance $R_{(P_{1i})}$, i = 1 to 7, between the boulder and the pressure cells when the impact begins. This initial distance is related to the horizontal distances between the vertical impact trajectory and pressure cells by equation 1:

$$R_{(P_{1i})} = \sqrt{D^2 + (r_{(P_{1i})})^2} \tag{1}$$

Where D is the protective layer thickness.

RESULTS

Figure 9 illustrates typical "induced pressure" versus time curves observed at the top of the SRC slab during an impact test. The term "induced pressure" designates the increment of pressure through the sand layer caused by the impact at the top of the layer, *i.e.* the total pressure observed in the pressure cells minus the sand layer's self-weight, a constant value that was observed in the pressure cells before performing the tests. This way, the value of induced pressure is initially equal to zero and, after a certain duration, it returns to zero again.

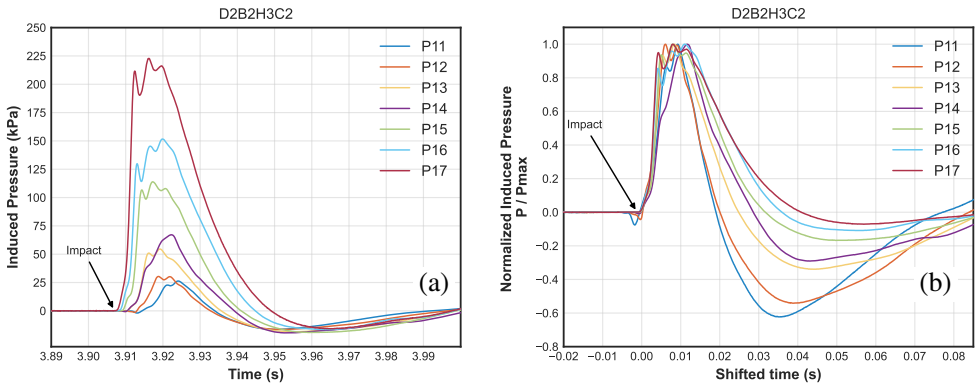

Fig. 9. Analysis of pressure cell measurements in test D2B2H3C2: (a) Induced pressure vs. time curves (a) and (b) Normalized induced pressure vs. shifted time.

As mentioned in the preceding, there was an offset between the targeted point at the surface of the sand layer (located above pressure cell P17) and the final position of the block. In this test (D2B2H3C2), the offset, presented in a plan view in a subsequent figure, was such that P17 was the pressure cell closest to the impact trajectory, leading to the maximum observed value of peak induced pressure in Figure 9 (a). P15 and P16 (see Figure 7 for the pressure cells numbering in the experimental setup) were located at about the same distance from the trajectory, some 50 cm farther, thus being subjected to similar but lower values of peak induced pressure. The typical results from Figure 9 (a) illustrate four aspects of the observed behavior, which will help to understand the data reduction procedure presented in the following. First, the moment where the pressure begins to rise in a pressure cell increases within the distance of the cell to the impact trajectory (in the figure, the lower the peak, the larger the distance). Second, the rate at which the pressure rises is lower for the more distant sensors. Third, in the graphs, local oscillations may be noted in the pressure measurements for all the cells. These local "high frequency" variations on the curves, of a few milliseconds period duration, were attributed to the natural vibration frequency of the pressure cells, which are protected from punching by two thick steel disks of 23 cm diameter (the first mode natural vibration frequency of a square steel plate of 20 cm long and 2.5 cm thick is about 500 Hz, *i.e.* 2 ms duration). Fourth, after a certain duration, the induced pressure may become negative before returning progressively to zero. In the D2B2H3C2 test, the sand layer thickness was 1.5 m.

The self-weight of the layer was of the order of 25 kPa. Therefore, the pressure applied at the top of the slab decreased due to the cushion layer's self-weight but remained positive (in compression). This phenomenon was related to the dynamic deflection of the slab, delayed of about 30 ms due to its inertia. In all the tests, the pressure remained positive at the sand-slab interface and no effect of possible subsequent vibration of the slab was observed.

Based on a large amount of cell pressure measurements, the purpose of the data reduction procedure detailed in the following is to represent, for each impact test, the space and time induced pressure pulse distribution using as few characteristic properties as possible. First, the data reduction procedure to represent the spatial distribution at the slab's surface of the induced pressure peak values is presented. Secondly, the representation of the induced pressure versus time at a specific distance from the impact trajectory is considered.

Spatial distribution of induced pressure peak values at the slab's surface

The peak of induced pressure, at different distances from the impact trajectory, is a key aspect to describe the time-space induced pressure pulse transmitted to the slab through the protective sand layer. As shown in Figure 9(a) for test D2B2H3C2, a maximum value of induced pressure may be observed during the impact for each pressure cell. In Figure 10(a), the maximum values of induced pressure at the seven pressure cells (P11 to P17) was plotted as a function of the distance from the center of the pressure cell to the impact trajectory (r_{P1i}). For test D2B2H3C2, Figure 10 (b) shows the locations of the impact point and of the pressure cells setup in the XY-plane, at the top of the slab. The distribution of induced pressure peak values had to be extrapolated towards the impact trajectory, at a distance r = 0, as shown on Figure 10 (a).

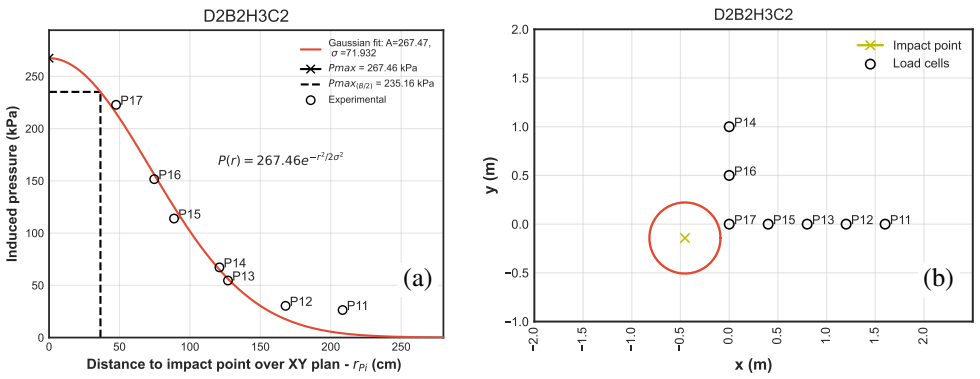

Fig. 10. (a) Induced peak pressure as a function of distance from impact point; and (b) Impact point on XY plane. (test 14, D2B2H3C2).

The large number of tests (35) was helpful to develop a good understanding of the shape of the induced pressure peak distribution about the impact trajectory. An axisymmetric distribution was confirmed by the measurements observed along the two lines of pressure cells, in the X and Y directions, which gave close values for cells at similar radial distances to the impact trajectory (r). The "bell-shape" of the observed peak values of induced pressure with the distance to the impact trajectory suggested to represent this spatial distribution using a normal distribution function described by Equation (2):

$$P_{max}(r) = P_{maxx} \cdot e^{-\beta r^2} \tag{2}$$

In the data reduction procedure applied to each test, the two parameters in Equation 2 (P_{maxx} and β) were determined by non-linear least squares fit (Levenberg 1944; Marquardt 1963). Physically, the P_{maxx} parameter in fact is the overall maximum value of induced pressure, occurring at r = 0, on the impact trajectory. The β parameter describes the decay of induced pressure peak values with increasing distance to the impact trajectory. Bearing in mind that the induced pressure spatial distribution might be related to the block size (thus the equivalent diameter B), it was decided to consider the peak value of induced pressure at a distance B/2 from the impact trajectory, *i.e.* right below the block's edge in the direction of impact. The peak value of induced pressure below block's

edge is thus expressed by the Equation 3:

$$P(B/2) = P_{maxx} \cdot e^{-\beta \cdot (B/2)^2} \tag{3}$$

Conversely, the normal distribution decay of induced pressure peak values with the distance to the impact trajectory (β) is related to the induced pressure peak value at the periphery of the block throughout the following Equation 4:

$$\beta = \frac{\ln(P_{maxx}/P_{max}(B/2))}{(B/2)^2} \tag{4}$$

In summary, the spatial distribution of peak values of induced pressure at the surface of the slab during the impact may be represented by Equation 2. This equation is based on two physical characteristic properties of the induced pressure pulse, P_{maxx} and β. The first one is the overall peak value of induced pressure, on the impact trajectory. The second one characterizes the decay of induced pressure peak values with increasing distance to the impact trajectory. This property was related to the decay of induced pressure peak values from the center to the periphery of the block in the direction of impact.

Time distribution of the induced pressure pulse

At a given distance from the impact trajectory, the induced pressure at the slab's surface during an impact on the protective soil layer starts to rise at a specific moment, then rapidly increases to a peak value and finally progressively returns to zero. In the following three sections, the tests results are analyzed regarding these three aspects. The purpose is still to identify characteristic properties which may be used to represent the time-space induced pressure pulse transmitted to the slab.

Pressure pulse delay at the sand-slab surface

Concerning the pressure pulse at the top of the slab during an impact, as illustrated in Figure 9(a), showing the induced pressure observed with the pressure cells, the time of impact does not coincide with the moment when the pressure begins to rise in the pressure cells. As a matter

of fact, a delay is observed between the moment of impact and when pressure begins to rise in the pressure cell. It may be noted that this delay increases with the distance of the pressure cell to the impact trajectory.

As a consequence, the signal from each pressure cell at the beginning of impact was treated to evaluate the exact moment when the pressure begins to increase, becoming larger than the constant unit weight of the soil layer measured before impact. At each cell, the beginning of the pressure pulse was defined as the moment when the measured pressure exceeds the constant initial pressure by 2.5 times the noise of the recorded signal from the pressure cell before impact. In terms of induced pressure, which was equal to zero before the impact, this moment is when the induced pressure becomes larger than 2.5 the noise in the signal from the pressure cell before impact.

By reference to the propagation of mechanical waves in an elastic media, in Figure 11, the moment when pressure begins to rise in the pressure cell $P_{(1i)}$, i = 1 to 7 (see Figure 8), was plotted versus the distance of the pressure cell to the impact point at the top of the layer, denoted $R(P_{(1i)})$ in Figure 8. Figure 11 shows that the time at which the pressure pulse begins at a pressure cell increases linearly with the distance of the pressure cell to the impact point at the top of the layer.

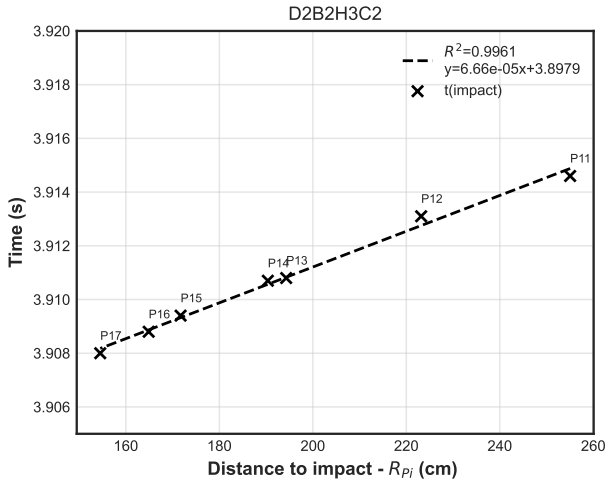

Fig. 11. Time when induced pressure pulse begins vs. distance to the impact point at the top of the protective soil layer (test D2B2H3C2).

The slope of this relationship may be interpreted as the stress propagation velocity through the

sand layer. This velocity is denoted as A_i. An important result from this study is that, in all the 35 tests, the same value of the A_i velocity was found, no matter the layer thickness, block size or impact speed. For the sand compacted in all the tests to the same density (1.53), this velocity was of the order of 150 m/s. Such a value is way below the usual velocity of compression wave (V_p) from seismic refraction geophysical tests in fine dry sands, which varies from 300 to 700 m/s for loose to dense sands. In fact, the loading conditions in the sand during impact, producing plastic flow and large strains and displacements, are such that the elastic behavior assumption does not apply. However, this physical phenomenon, characterized by a constant value of the A_i velocity, independent of the impact factors D, B and V, is an useful information to represent the space-time pressure pulse at the surface of the slab during a rockfall impact. The time at which the pressure on the protected slab begins to increase at a distance r from the impact trajectory at the soil-slab's interface may be expressed by Equation 5:

$$t_i(r) = t_i(0) + \frac{\sqrt{D^2 + r^2} - D}{A_i} \tag{5}$$

In which $t_i(0)$ is the "initial" moment, when the pressure at the point on the slab surface corresponding to the impact trajectory (r = 0 and R = D) begins to increase. During the tests, the pressure cells measurements were recorded in function of time. It may be noted that the moment corresponding to t_i (0) may be defined in Figure 11 by extrapolating the linear relationship back, towards R = D, *i.e.* r = 0. This moment may be used to define a new time origin, meaning that $t_i(0) = 0$. With this convention, for the origin of time, the pressure pulse induced by the impact would begin in r = 0 cm and at time t = 0 s.

Induced pressure increase rate

The moment at which the induced pressure reaches its peak value at a pressure cell location, at a distance r from the impact trajectory, is an important information to describe the pressure pulse caused by the impact. In fact, it governs the loading rate, which is fundamental in dynamic structural design. Unfortunately, as illustrated in Figure 9 a), presenting the induced pressure observed

during impact in the seven pressure cells for test D2B2H3C2, the moment at which the pressure pulse reaches the peak value at a pressure cell location cannot be accurately determined due to local oscillations. In an attempt to estimate whether the time to peak pressure depends on the distance to the impact trajectory, it was decided to plot the "normalized" induced pressure, *i.e.* the induced pressure divided by its maximum value during the impact. In addition, to properly compare the pressure increase duration at each pressure cell, for each normalized induced pressure curve, the value of time was shifted by t_i (r), the delay between the impact time and the moment where the pressure begins to rise at the pressure cell. Figure 9 shows, for the test D2B2H3C2, (a) the observed induced pressure versus time at the different pressure cell locations and (b) the corresponding normalized induced pressure versus time shifted by t_i (r). The larger negative values of normalized induced pressure, up to -0.6 at P11 pressure cell, correspond to the farthest pressure cells, where the peak values of induced pressure are the lowest, of the order of the unit weight of the protective fill. As explained earlier, the negative values of induced pressure is related to the dynamic deflection of the thick SRC slab. From Figure 9, it clearly appears that, during pressure increase, the normalized induced pressure versus shifted time curves overlap. The same physical phenomenon was systematically observed in all the 35 tests: the rate of increase of normalized induced pressure is therefore independent to the distance to the impact trajectory (r). This important physical phenomenon means that the expression for the pressure on the slab induced by an impact is of the general following form described by Equations 6, 7 and 8:

For $t \leq t_i(r)$:

$$P(r,t) = 0 \tag{6}$$

For $t_i(r) \leq t < t_{max}(r)$:

$$P(r,t) = P_{max}(r) \cdot f(t - t_i(r)) \tag{7}$$

and for $t \geq t_{max}(r)$:

$$P(r,t) = P_{max}(r) \cdot g(r, t - t_{max}) \tag{8}$$

In which t_{max}(r) is the time where the induced pressure reaches its maximum value at a distance

r from the impact trajectory. P_{max}(r), the maximum value of induced pressure at a distance r from the impact trajectory, was expressed in Equation 2 in terms of two characteristic properties of the pulse of induced pressure, P_{maxx} (the overall maximum induced pressure, on the impact trajectory) and β (defining the normal distribution of induced pressure peak values with distance to the impact trajectory). While the induced pressure increases to its peak value (Equation 7), the normalized induced pressure is only a function of time (function f in Equation 7). However, while the pressure decreases, the normalized induced pressure is a function of both time and distance to the impact trajectory (function g in Equation 8).

Unfortunately, it may also be pointed out from Figure 9 that, due to the local oscillations in the pressure cells measurements, such a representation of the test's results does not help to determine the time at which the peak of pressure occurs at the different pressure cell locations. As a consequence, to represent the induced pressure pulse prior to its peak value at a distance r from the impact trajectory (i.e. to define the f function in Equation 7), the most reliable approach was to consider the time-rate increase of normalized induced pressure, which is the same at any point on the slab. In each test, only a few pressure cells measurements were affected by local oscillations during pressure increase, like P14 in test D2B2H3C2 (see Figure 9). In the data reduction process, the measurements from these pressure cells produced results which were obviously inconsistent with others.

The time-rate increase of normalized induced pressure, prior to peak value, was therefore assumed to be characterized by the slope of the normalized induced pressure versus shifted time curve at 50% of the peak value, denoted p_{50}. As may be noticed in Figure 12, the value of this slope p_{50}, away from the start of the curve at $t - t_i$ and from the oscillations near the peak, is a reliable characteristic property of all the curves. It is a representative property of the rate of loading on the protected slab during the impact.

In Figure 9 (b), the shape of the curves prior to peak led to represent the normalized induced pressure versus shifted time (the f function) with a parabolic relationship based on three properties of the curves: *(i)* Its value is zero at time t_i, *(ii)* Slope is p_{50} when the value is 0.5 and *(iii)* Slope

is zero at the top, where the value is 1 (at the peak). Such a parabolic f function is represented in Figure 12.

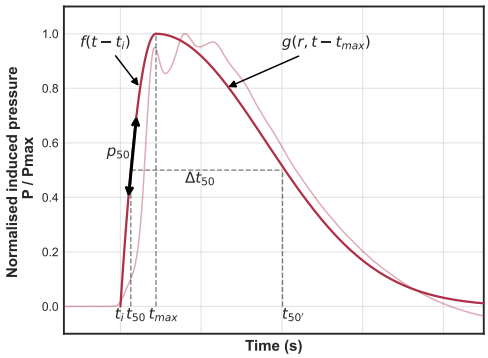

Fig. 12. Representation of the normalized induced pressure vs. time.

The parabolic function representing the relationship between normalized induced pressure vs. time before peak pressure is given by the following Equation 9:

$$f(t - t_i(r)) = -\frac{(p_{50})^2}{2} \cdot (t - t_i(r))^2 + \sqrt{2} \cdot (p_{50}) \cdot (t - t_i(r)) \tag{9}$$

For each impact test the characteristic property p_{50} was obtained from the data reduction procedure applied to the pressure cells measurements. The value of t_i (r) , the time at which the pressure starts to increase at a distance r from the impact trajectory on the slab was given by Equation 5 in the preceding.

The previous equation may be used to calculate the time t_{max} at which the induced pressure reaches its maximum at a distance r from the impact trajectory (Equation 10):

$$t_{max}(r) = \frac{\sqrt{2}}{p_{50}(r)} + t_i(r) \tag{10}$$

Similarly, the time t_{50} at which 50% of the maximum induced pressure occurs (corresponding to the point where the slope p_{50} is determined), is given by the following Equation 11:

$$t_{50}(r) = \frac{\sqrt{2} - 1}{p_{50}} + t_i(r) \tag{11}$$

Pulse duration and induced pressure unloading rate

To complete the description of the pressure pulse at a distance r from the impact trajectory, the decrease of normalized induced pressure versus time after the peak, *i.e.* the *g* function in Equation 8, has to be characterized. In fact, for dynamic structural design, the unloading rate is as important as the loading rate. Considering the pressure measurements, defining the duration of unloading after the peak of pressure did not appear to be the most effective approach to characterize the unloading rate, since the induced pressure rapidly drops after the peak and very progressively returns to zero (see Figure 9(a)). Besides, the dynamic behavior of the slab impaired the measurements for the larger times after impact (larger than about 30 ms after impact). In addition, as explained in the preceding, the local oscillations in the pressure measurements did not allow to precisely identify the time at which the induced pressure reaches its maximum at a distance r from the impact trajectory (t_{max}(r)). Therefore, the most effective approach to evaluate the unloading rate appeared to be relying on the time during which the pressure is greater than 50% of its peak value (or normalized induced pressure greater than 0.5). This duration, represented in Figure 12, was denoted Δt_{50}. The local oscillations in the measurements while pressure is initially rising and after peak decreasing may introduce some uncertainties in the determination of Δt_{50} for some of the pressure cells. However, this data reduction process turned out to produce consistent and reliable values of Δt_{50}.

As illustrated by the graph in Figure 9(b), the duration of the normalized induced pressure pulse depends on the distance to the impact trajectory. The closer to the impact trajectory (pressure cell P17), the longer the pulse duration. To investigate this relationship, the values of Δt_{50} from the seven pressure cells were plotted versus the distance to the impact trajectory (r). Figure 13 shows this graph for test D2B2H3C2.

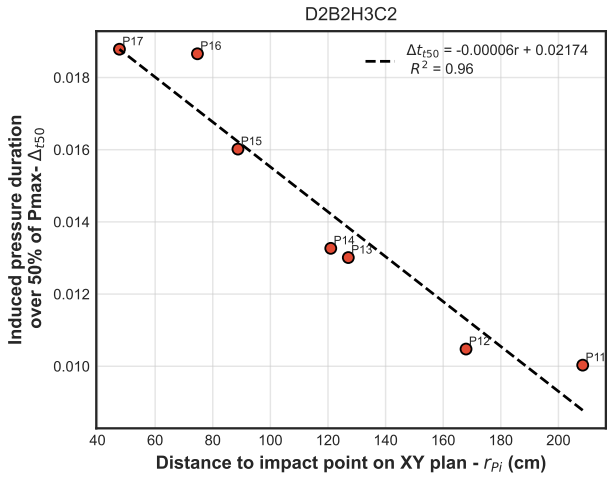

Fig. 13. Time duration on which the pressure is greater than 50% of peak value in the pressure cells at different distances to the impact trajectory (test D2B2H3C2).

Such a linear relationship was consistently observed in all the 35 impact tests. Thus the value of Δt_{50} at a distance r from the impact trajectory may be expressed as follows (Equation 12):

$$\Delta t_{50} = \Delta t_{50}(r = 0) - \frac{r}{A_{50}} \tag{12}$$

Where Δt_{50} (0) represents the time during which the induced pressure, on the impact trajectory, remains larger than 50% of its peak value. A_{50} is the inverse value of the slope of the linear relationship of the graph in Figure 13. It has the dimension of a velocity.

For each impact test, the y-intercept Δt_{50} (0) and the slope inverse A_{50} are two characteristic properties of the space-time pressure pulse transmitted to the structure during the impact on the protective soil layer. The results of the linear regression at the top of the graph in Figure 13 indicate that, for test D2B2H3C2, Δt_{50} (0) was 21.74 ms and A_{50} about 165 m/s.

The shape of the normalized induced pressure curve after the peak and its progressive decrease to zero suggest to consider for the g function a Gaussian function, centered at the peak, where $t = t_{max}$. At this point, the derivatives of both expressions for the pressure pulse, before the peak (function f) and after the peak (function g), are zero. Consequently, the g function was given the following form (Equation 13):

For $t \geq t_{max}$(r):

$$g_{(r,t)} = e^{-\gamma_{(r)} \cdot (t - t_{max}(r))^2} \tag{13}$$

In which γ(r) is the normalized induced pressure decay rate beyond the peak, which depends on the distance r to the impact trajectory.

At a distance r from the impact trajectory, the decay of normalized induced pressure beyond the peak (γ(r)) is in fact related to the duration of the pressure pulse, which may be represented by the duration Δt_{50} (r). Noting that the g function in Equation 13 equals 1/2 when time is equal to t_{50}(r) plus Δt_{50} (r), and substituting t_{max} (r) by its expression in Equation 10 and t_{50}(r) in Equation 11, the following expression for γ(r) may be derived on Equation 14:

$$\gamma_{(r)} = \frac{\ln(2) \cdot {p_{50}}^2}{(p_{50} \cdot \Delta t_{50}(r) - 1)^2} \tag{14}$$

Where p_{50}, the rate of increase of the normalized induced pressure before peak, was defined in the preceding and Δt_{50} (r), the duration of the pressure pulse above 50% of its maximum, is given by Equation 12. p_{50} is a characteristic property of the induced pressure pulse, as well as Δt_{50} (0) and A_{50} in Equation 12.

CONCLUSION

A total of 35 instrumented tests were performed, with sand layer up to 2 m thick, rock boulder size up to 1.78 m (mass 7399 kg) and impact velocity up to 91 km/h. The sand layer construction procedure was the same for all the tests and the sand's dry density was 1.53. The pressure transmitted through the protective sand layer during the impact was observed using pressure cells located on the structure at several distances from the impact trajectory. The analysis of tests results allowed to observe several physical phenomena, which were then employed to identify characteristic properties defining the space-time pressure pulse at the surface of the structure induced by the impact on the sand layer.

Physical phenomena may be observed. First, the time at which the pressure induced by the impact at the surface of the structure begins to rise, denoted t_i (r), increases linearly with the distance

to the impact point at the top of the protective layer (R), defining an "initial propagation velocity" of the induced pressure. The same value of initial propagation velocity (A_i) was observed in all the tests. This characteristic property was thus fond independent of D, B and V. It may however pertain to the sand's grain size distribution and dry density, which were constant in all tests.

Second, the time-rate increase of the normalized induced pressure (the pressure divided by its maximum value during impact) was observed to be independent of the distance to the impact trajectory. This physical phenomenon implies that, during pressure increase, the space and time variables may be separated in the expression for p(r,t),as represented by Equation 7.

The maximum induced pressure value ($P_{max}(r)$) was represented by a Gaussian distribution, centered on the impact trajectory (r = 0). The distribution was then defined by the two following characteristic properties: the maximum induced pressure on the impact trajectory (P_{maxx}) and the decay rate β, which was related the maximum induced pressure value observed at the block's periphery: $P_{max}(r = B/2)$.

Two functions, f and g, were defined to represent the normalized induced pressure as function of time, respectively during pressure increase and decrease. The function f does not depend on the distance to the impact trajectory. These two functions were defined using three additional characteristic properties of the normalized induced pressure pulse:

1. p_{50}: The time-rate of increase of normalized induced pressure when the pressure reaches 50% of its peak value, which was found to be independent of r.
2. Δt_{50} (0): The duration of time while the induced pressure on the impact trajectory remains larger than 50% of its peak value.
3. A_{50}: A velocity which describes the linear decrease of Δt_{50} (r) with the distance to the impact trajectory (r). In other words, the decrease of the duration of the normalized induced pressure pulse with the distance to impact trajectory. This velocity was related to the value Δt_{50} (B/2).

The values of the five characteristic properties of the induced pressure pulse (P_{maxx}, β, p_{50}, $\Delta t_{50}(0)$

and A_{50}) for the 35 impact tests have been gathered in Appendix I, Table 3. For each impact test condition D, B and V, the induced pressure pulse at the slab surface during the impact may be represented using the expressions for P_{max} (r) , f and g and computed with the corresponding characteristic properties in Appendix I, Table 4. In practice, considering a rockfall hazard defined as a block of equivalent diameter B and an impact velocity V, and assuming a protective sand layer of thickness D, an approximate induced space-time pressure pulse distribution p(r,t) at the surface of the protected structure may already be estimated selecting the appropriate properties values in Table 4.The structure subjected to such a space-time pressure pulse may then be designed in dynamic conditions as explained for example by Kappos (2002).

It may be assumed that the approach presented in this study to define the space-time pressure pulse distribution overestimates the actual pressure pulse for two reasons. First, the tests were performed on a very stiff structure (a concrete slab 60 cm thick cast in place on a rock substratum). Should a more flexible structure be considered, lower induced pressure values would have been observed. Second, in this study, the impact was perpendicular to the protected structure. For a lower impact angle, the induced pressure values would probably be lower, since a larger mass of the soil layer would be displaced. However, it must be emphasized that this approach does not apply for any block shape. For an elongated block shape, the impact on a sharp edge or the smallest side will lead to deeper penetration, larger peak and narrower spatial distribution of induced pressure.

NOTATION

The following symbols are used in this paper:

D = Sand cushion layer thickness (m);

B = Block's diameter (m);

H = Release Height (m) ;

V = Impact Speed (m/s);

d = Block's characteristic dimension (m) ;

w = Steel-reinforced concrete slab thickness (m);

Appendix I. EXPERIMENTAL TEST REFERENCING

Table 3. Experimental tests referencing for given impact coordinates (x and y)

Test (ref)	D (ref)	B (ref)	H (ref)	X_{impact} (cm)	Y_{impact} (cm)
1	1	1	1	-16.22	5.92
2	1	1	2	-42.01	27.50
3	1	1	3	-52.31	-9.99
4	1	1	4	-68.52	-9.51
5	1	2	1	-6.45	-3.30
6	1	2	2	-10.96	0.57
7	1	2	3	-11.49	3.59
8	1	2	4	-19.89	8.46
9	2	1	1	-25.27	-12.20
10	2	1	2	-23.43	-13.47
11	2	1	3	-43.14	-17.05
12	2	1	4	-32.77	-15.16
13	2	2	1	-25.17	-18.58
14	2	2	2	-45.58	-5.99
15	2	2	3	-45.78	-14.23
16	2	2	4	-45.78	-14.23
17	2	4	1	-22.99	18.05
18	2	4	2	-44.52	0.70
19	2	4	3	-16.70	-9.10
20	2	4	4	-12.52	-2.14
21	2	5	1	-69.94	0.17
22	2	5	2	-44.01	20.14
23	2	5	3	-32.07	-3.78
24	2	5	4	-24.92	-42.87
25	1	4	1	-21.23	20.72
26	3	5	4	-10.87	-4.04
27	3	5	3	-19.50	16.83
28	3	1	1	-34.97	6.75
29	3	1	2	-33.88	23.05
30	3	1	3	-42.70	15.51
31	3	1	4	-38.80	59.41
32	3	2	1	-23.63	0.33
33	3	2	2	-20.68	-13.69
34	3	4	5	-25.76	0.01
35	3	3	3	-7.92	12.08

Table 4. Summary of the characteristic properties of the space-time induced pressure pulse distribution for the 35 tests.

Test (ref)	D (cm)	B (m)	B/D	H (m)	Impact Speed (m/s)	Impact Speed (km/h)	P_{maxx} (kPa)	β	$p50$ (s^{-1})	$\Delta t_{50}(0)$ (ms)	A_{50} (m/s)	$P_{(B/2)}$ (kPa)	$\Delta t_{50}(B/2)$ (ms)
1	100	0.42	0.42	1	4.43	15.95	22.09	1.15×10^{-4}	729.29	23.80	46.87	21.00	19.30
2	100	0.42	0.42	5	9.90	35.66	48.37	1.52×10^{-4}	804.31	29.30	58.86	45.23	25.70
3	100	0.42	0.42	10	14.01	50.43	74.32	1.31×10^{-4}	253.76	17.90	184.64	70.13	16.80
4	100	0.42	0.42	20	19.81	71.31	176.36	1.16×10^{-4}	671.37	10.20	1130.59	167.58	10.00
5	100	0.73	0.73	1	4.43	15.95	77.81	2.62×10^{-4}	95.12	37.40	76.83	54.89	32.60
6	100	0.73	0.73	5	9.90	35.66	217.17	1.97×10^{-4}	480.34	27.90	91.72	166.93	23.90
7	100	0.73	0.73	10	14.01	50.43	348.49	2.05×10^{-4}	455.38	22.80	83.87	265.19	18.40
8	100	0.73	0.73	20	19.81	71.31	705.07	1.96×10^{-4}	741.09	21.30	83.23	542.91	16.90
9	150	0.42	0.28	1	4.43	15.95	8.51	7.04×10^{-5}	541.78	23.20	146.15	8.25	21.80
10	150	0.42	0.28	5	9.90	35.66	32.28	5.86×10^{-5}	752.03	20.40	119.68	31.46	18.60
11	150	0.42	0.28	10	14.01	50.43	46.79	5.12×10^{-5}	284.74	19.30	162.84	45.75	18.00
12	150	0.42	0.28	20	19.81	71.31	82.86	6.55×10^{-5}	274.45	13.40	318.87	80.50	12.70
13	150	0.73	0.49	1	4.43	15.95	39.76	1.06×10^{-4}	570.87	38.90	69.11	34.52	33.60
14	150	0.73	0.49	5	9.90	35.66	104.26	7.98×10^{-5}	364.88	30.70	97.50	93.74	26.90
15	150	0.73	0.49	10	14.01	50.43	267.47	9.66×10^{-5}	320.71	21.70	160.79	235.16	19.50
16	150	0.73	0.49	20	19.81	71.31	341.45	7.70×10^{-5}	574.15	20.30	153.76	308.17	17.90
17	150	1.58	1.05	1	4.43	15.95	288.61	1.42×10^{-4}	294.51	53.70	40.06	118.97	34.00
18	150	1.58	1.05	5	9.90	35.66	757.12	1.04×10^{-4}	743.89	39.60	111.36	394.95	32.50
19	150	1.58	1.05	10	14.01	50.43	944.76	1.04×10^{-4}	89.63	36.40	112.24	492.34	29.40
20	150	1.58	1.05	20	19.81	71.31	2127.05	1.17×10^{-4}	149.66	30.40	108.41	1021.69	23.10
21	150	1.79	1.19	1	4.43	15.95	401.00	9.24×10^{-5}	106.85	58.70	52.39	191.32	41.60
22	150	1.79	1.19	5	9.90	35.66	1041.78	1.19×10^{-4}	212.84	41.10	109.33	401.03	32.90
23	150	1.79	1.19	10	14.01	50.43	1203.58	9.19×10^{-5}	170.08	45.00	82.61	576.37	34.20
24	150	1.79	1.19	20	19.81	71.31	3006.73	1.11×10^{-4}	451.01	39.10	71.35	1236.87	26.50
25	100	1.58	1.58	1	4.43	15.95	553.83	2.34×10^{-4}	318.49	47.80	47.65	128.81	31.20
26	200	1.79	0.90	20	19.81	71.31	1259.98	6.06×10^{-5}	370.58	38.40	113.92	775.18	30.60
27	200	1.79	0.90	10	14.01	50.43	968.65	4.61×10^{-5}	362.37	39.20	103.59	669.62	30.60
28	200	0.42	0.21	1	4.43	15.95	8.17	3.25×10^{-5}	558.66	11.90	2575.99	8.06	12.00
29	200	0.42	0.21	5	9.90	35.66	28.21	4.11×10^{-5}	526.32	15.00	437.80	27.70	14.50
30	200	0.42	0.21	10	14.01	50.43	49.84	4.60×10^{-5}	284.94	14.10	491.81	48.84	13.60
31	200	0.42	0.21	20	19.81	71.31	74.67	3.75×10^{-5}	422.05	12.80	526.68	73.44	12.40
32	200	0.73	0.37	1	4.43	15.95	20.53	3.75×10^{-5}	159.43	39.30	72.11	19.53	34.20
33	200	0.73	0.37	5	9.90	35.66	86.49	4.89×10^{-5}	303.21	20.40	233.79	81.04	18.90
34	200	1.58	0.79	33	25.45	91.60	2165.61	6.87×10^{-5}	494.10	37.60	84.04	1410.47	28.20
35	200	0.73	0.37	10	14.01	50.43	641.00	6.10×10^{-5}	140.45	38.00	90.31	590.98	34.00

References

ASTRA – Swiss Federal Transportation Office (2008). *Actions de chutes de pierres sur les galeries de protection.*

Bhatti, A. (2015). "Falling-weight impact response for prototype rc type rock-shed with sand cushion.." *Mater Struct*, 48, 3367–3375.

Calvetti, F. and Di Prisco, C. (2012). "Rockfall impacts on sheltering tunnels: real-scale experiments." *Géotechnique*, 62(10), 865–876.

Calvetti, F. and Vecchiotti, M. (2005). "Experimental and numerical study of rock-fall impacts on granular soils." *Rivista Italiana di Geotecnica*, 4.

Durville, J. L., Guillemin, P., Berthet Rambaud, P., and Subrin, D. (2010). *Etat de l'art sur le dimensionnement des dispositifs de protection contre les chutes de blocs*. Laboratoire Central des Ponts et Chaussées (LCPC), <https://hal.archives-ouvertes.fr/hal-00508901> (January).

Heidenreich, B. (2004). "Small-and half-scale experimental studies of rockfall impacts on sandy slopes." *Report no.*, EPFL.

Japan Road Association (2000). *Rockfall Countermeasure Handbook (in Japanese)*.

Kappos, A. (2002). *Dynamic loading and design of structures*. Spon Press, London.

Kishi, N., Konno, H., Ikeda, K., and Matsuoka, K. (2002). "Prototype impact tests on ultimate impact resistance of pc rock-sheds." *International Journal of Impact Engineering*, 27(9), 969–985.

Labiouse, V., Descoeudres, F., and Montani, S. (1996). "Experimental study of rock sheds impacted by rock blocks." *Structural Engineering International*, 6(3), 171–176.

Levenberg, K. (1944). "A method for the solution of certain non-linear problems in least squares." *Quarterly of applied mathematics*, 2(2), 164–168.

Marquardt, D. W. (1963). "An algorithm for least-squares estimation of nonlinear parameters." *Journal of the society for Industrial and Applied Mathematics*, 11(2), 431–441.

Montani Stoffel, S. (1998). "Sollicitation dynamique de la couverture des galeries de protection lors de chutes de blocs." Ph.D. thesis, EPFL, Lausanne, <http://infoscience.epfl.ch/record/32376>.

Oussalah, T. (2018). "Comportement des sables sous sollicitation d'impact à faible vitesse : ap-

plication au dimensionnement de couches de sol protégeant les structures des impacts rocheux." Ph.d. thesis, Université de Lyon, France, <https://tel.archives-ouvertes.fr/tel-01923593>.

Pichler, B., Hellmich, C., and Mang, H. (2005). "Impact of rocks onto gravel design and evaluation of experiments." *International Journal of Impact Engineering*, 31(5), 559–578.

Schellenberg, K. (2008). "On the design of rockfall protection galleries." Ph.D. thesis, ETH Zurich, Switzerland.

Yoshida, H., Masuya, H., and Ihara, T. (1988). "Experimental study of impulsive design load for rock sheds." *IABSE proceedings*, 3, 61–74.